Dynamical relaying can yield zero time lag neuronal synchrony despite long conduction delays

Raul Vicente[a,b,1], Leonardo L. Gollo[c], Claudio R. Mirasso[c], Ingo Fischer[d], and Gordon Pipa[a,b,e,f]

[a]Department of Neurophysiology, Max Planck Institute for Brain Research, Deutschordenstrasse 46, 60528 Frankfurt, Germany; [b]Frankfurt Institute for Advanced Studies, Ruth-Moufang-Strasse 1, 60438 Frankfurt, Germany; [c]Instituto de Física Interdisciplinar y Sistemas Complejos, Universidad de las Islas Baleares-Consejo Superior de Investigaciones Cientificas, Campus Universidad de las Islas Baleares, E-07122, Palma de Mallorca, Spain; [d]School of Engineering and Physical Science and Joint Research Institute for Integrated Systems, Heriot–Watt University, Edinburgh EH14 4AS, Scotland; [e]Department of Brain and Cognitive Sciences, Harvard/Massachusetts Institute of Technology Division of Health Science and Technology, Massachusetts Institute of Technology, 77 Massachusetts Avenue, Cambridge, MA 02139-4307; and [f]Department of Anesthesia and Critical Care, Massachusetts General Hospital, 55 Fruit Street, Gray–Bigelow 4, Boston, MA 02114-2696

Communicated by Rodolfo R. Llinás, New York University Medical Center, New York, NY, September 18, 2008 (received for review June 11, 2008)

Multielectrode recordings have revealed zero time lag synchronization among remote cerebral cortical areas. However, the axonal conduction delays among such distant regions can amount to several tens of milliseconds. It is still unclear which mechanism is giving rise to isochronous discharge of widely distributed neurons, despite such latencies. Here, we investigate the synchronization properties of a simple network motif and found that, even in the presence of large axonal conduction delays, distant neuronal populations self-organize into lag-free oscillations. According to our results, cortico–cortical association fibers and certain cortico–thalamo–cortical loops represent ideal circuits to circumvent the phase shifts and time lags associated with conduction delays.

thalamocortical system | isochronous oscillations | phase locking | long-range synchronization | axonal latency

Cells in the visual cortex of mammals tend to fire simultaneously when activated by related features of a visual stimulus (1–4). This observation provided some of the early evidence that the nervous system may use an internal temporal code to process information. Since then, multicell electrophysiological studies have revealed the synchronous discharge of neurons distributed in different structures of the cerebral cortex, hippocampal formation, and thalamus (5, 6). Its biological significance derives from the observation that such precise and coordinated spike timing correlates with perception and behavioral performance (7–10). Remarkably, synchrony of neuronal activity is not limited to short-range interactions within a cortical patch. Interareal synchronization across cortical regions including interhemispheric areas has been observed in several tasks (7, 9, 11–14). The topological specificity and temporal unfolding of the synchrony reported in such studies are in agreement with its assumed role of subserving the effective "coupling" of the neuronal dynamics of the respective regions (9, 15).

Beyond its functional relevance, the zero time lag synchrony among such distant neuronal ensembles must be established by mechanisms that are able to compensate for the delays involved in the neuronal communication. Latencies in conducting nerve impulses down axonal processes can amount to delays of several tens of milliseconds between the generation of a spike in a presynaptic cell and the elicitation of a postsynaptic potential (16). The question is how, despite such temporal delays, the reciprocal interactions between two brain regions can lead to the associated neural populations to fire in unison.

Direct cortico–cortical fibers are major pathways of transareal communication and thus one principal substrate for the establishment of long-range synchrony. For instance, severing the corpus callosum was observed to disrupt the interhemispheric synchrony among homotopic cortical areas 17 in the cat (17). However, it is not clear whether direct excitatory cortico–cortical connections alone can mediate the zero phase synchronization of reciprocally coupled neurons for long transmission delays (18, 19). Several mechanisms have been pointed out as partially responsible for the enhancement of such synchrony. Inhibitory synapses and gap junctions have been proposed to stabilize the synchronous firing of cells under some specific conditions and for a limited range of delays (20, 21). In the case of the hippocampus, a canonical circuit of excitatory and inhibitory neurons have been shown to reproduce successfully the experimental findings of long-range synchrony among hippocampal neurons (5, 22, 23). Synaptic plasticity mechanisms have also been shown to stabilize synchronous γ oscillations between distant cortical areas by reinforcing the connections the delay of which matches the period of the oscillatory activity (24).

Nevertheless, significant long-range synchronization is observed across different species with different brain sizes and at different stages of the developmental growth of brain structures. This requires that any generic mechanism for generating zero time lag long-distance cortical synchrony maintains its functionality for a wide range of axonal lengths. Although it is possible that developmental mechanisms compensate for the resulting delay variations (25), it is still difficult to explain all of the phenomenology of long-distance synchronization without a mechanism that inherently allows for zero lag synchronization for a broad range of conduction delays and cell types.

In this paper, we investigate a simple network motif (26) that naturally accounts for the zero lag synchrony among two arbitrarily separated neuronal populations. We want to stress the separation of processes generating local rhythms or oscillations in a brain structure from the mechanisms responsible for their mutual synchronization. The model that we present below provides a proof of principle for a synchronizing mechanism among remote neuronal resources despite long axonal delays. The basic idea is that when two neuronal populations relay their activities to a third mediating population, the redistribution of the dynamics performed by this unit leads to a robust and self-organized zero lag synchrony among the outer populations (27, 28). Even if no particular brain structure or physiological condition is intended to be faithfully reproduced, this type of connectivity pattern is characteristic for the reciprocal interaction of different cortical areas and the associative thalamic nuclei, such as the pulvinar (29, 30), and as we shall show below it can give rise to isochronous dynamics in remote cortical populations. To demonstrate this effect, we conducted extensive simula-

Author contributions: R.V., L.L.G., C.R.M., I.F., and G.P. designed research; R.V., L.L.G., C.R.M., I.F., and G.P. performed research; R.V. and L.L.G. analyzed data; and R.V., L.L.G., C.R.M., I.F., and G.P. wrote the paper.

The authors declare no conflict of interest.

Freely available online through the PNAS open access option.

[1]To whom correspondence should be addressed. E-mail: raulvicente@mpih-frankfurt.mpg.de.

This article contains supporting information online at www.pnas.org/cgi/content/full/0809353105/DCSupplemental.

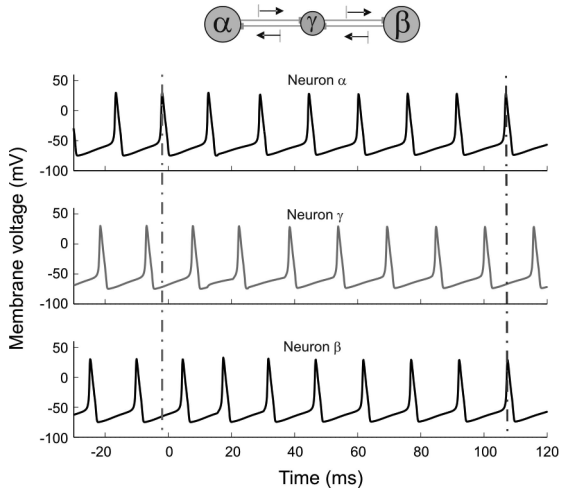

Fig. 1. Time series of the membrane voltage of 3 coupled HH cells N_α-N_β-N_γ. At time $t = 0$ the excitatory synapses were activated. Conduction delay $\tau = 8$ ms. Vertical lines help the eye to compare the spike synchrony before and after the interaction takes place.

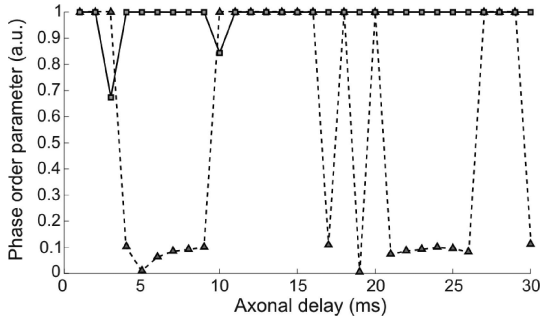

Fig. 2. Dependence of zero time lag synchronization as a function of the axonal delay between neighbor cells for a scheme of 2 coupled neurons (dashed line) and 3 coupled neurons (solid line). In the case of the 3 interacting cells, only the synchrony between the outer neurons is plotted here.

tions with networks of Hodgkin–Huxley (HH) neurons and integrate and fire (IAF) models to characterize the influence of long conduction delays in the synchronizing properties of this network module.

Results

Zero Time Lag Synchronization of Individual Neurons as a Self-Organization Process. We started by studying the spiking dynamics of a circuit composed of 3 HH cells with reciprocal delayed synaptic connections (for a schematic representation of the network architecture, see Fig. 1 *Top*). To inspect the role of such connectivity in synchronizing distant neurons we considered a configuration in which the isolated neurons had already an intrinsic spiking dynamics and observed how the synaptic activity modified the timing of their action potentials. By adding intracellular constant current stimulation (10 μA/cm^2), each isolated neuron developed a tonic firing mode with a natural period of 14.7 ms. The initial phase of the oscillations of each cell was randomly chosen to exclude trivial coherent effects. Finally, all axonal conduction delays were set to a considerably long value of 8 ms. Fig. 1 shows the evolution of the membrane potentials under such conditions when excitatory synaptic coupling among the cells is activated [see supporting information (SI) *Materials and Methods* for further details].

Before the coupling is switched on, the 3 cells fire out of phase as indicated by the left vertical guide to the eye in Fig. 1. However, once the interaction between the 3 neurons becomes effective at $t = 0$, a self-organized process, in which the outer neurons synchronize their spikes at zero lag even in the presence of long conduction delays, is observed. Notice that no external agent or influence is responsible for the setting of the synchronous state, but this is entirely negotiated by the network itself.

This mechanism of synchronization rests on the ability of an excitatory postsynaptic potential (EPSP) to modify the firing latencies of a postsynaptic neuron in a consistent manner. It further relies on the symmetric relay that the central neuron provides for the indirect communication between the outer neurons. The key idea is that this network motif allows for the outer neurons to exert an influence on each other via the intermediate relay cell. Thus, the reciprocal connections from the relay cell assure that the same influence that is propagating from one extreme end of the network to the other is also fed back into the neuron that originated the perturbation promoting the synchronous state. It must be noticed, however, that a pair of identical EPSPs elicited simultaneously on the outer neurons does not have in general an identical effect on both neurons. Actually, the effect of a postsynaptic potential on a neuron strongly depends on the internal state of the receiving cell, and more specifically on the phase of its spiking cycle at which the PSP is arriving (31–33). Because the neurons are in general at different phases of their oscillatory cycles, the effects of the EPSPs (magnitude and direction of the induced phase shifts) are different for the 3 cells. Nevertheless, the accumulation of such corrections to the interspike intervals of the outer neurons is such that after receiving a few EPSPs they compensate the initial phase difference, and both cells end up discharging isochronously, representing a stable state (see *SI Materials and Methods*). Our simulations also show that a millisecond-precise locking of spikes can be achieved already after the exchange of only a few spikes in the network.

A key issue of the synchronization properties exhibited by such network architecture is whether the zero lag correlation can be maintained for different axonal lengths or whether it is specific to a narrow range of axonal delays. Fig. 2 displays the quality of the zero lag synchronization between 2 HH neurons as a function of the conduction delays. Two scenarios were studied: one in which the neurons were directly coupled via excitatory synapses (dashed line) and a second one in which the 2 neurons interacted through a relay cell also in an excitatory manner (solid line). The synchronization index is given by the order parameter defined in the *SI Materials and Methods*. A value of 1 (zero) of this index indicates perfect synchrony (uncorrelation) at zero lag. A quick comparison already reveals that whereas the direct excitatory coupling exhibits large regions of axonal conduction delays where the zero lag synchrony is not achieved, the relay-mediated interaction leads to zero time lag synchrony in 28 of the 30 delay values explored (1–30) ms. Only for $\tau \approx 3$ ms and $\tau \approx 10$ ms, the 3 cells entered into a chaotic firing mode in which the neurons neither oscillated with a stable frequency nor exhibited a consistent relative lag between their respective spike trains. See also Fig. S1 for a description of the phase relations among the 3 neurons as a function of the axonal delay.

Robust zero lag synchrony among the outer neurons was also observed when the synaptic interaction between the cells was inhibitory instead of excitatory. Different synaptic rise and decay times within the typical range of fast AMPA- and $GABA_A$-mediated transmission were tested with results identical to those reported above. These results indicate that the network motif of 2 neurons relaying their activities through a 3rd neuron leads to a robust zero lag synchrony almost independently of the delay times and sign of the synaptic interactions. We also conducted simulations to test the robustness of this type of synchrony with respect to the

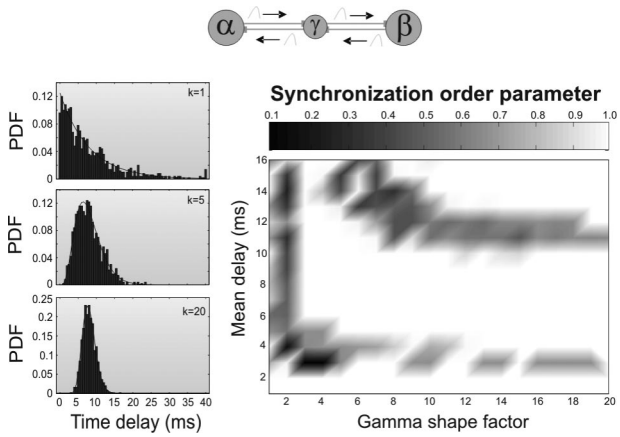

Fig. 3. Effects of broad distributions of axonal delays on synchrony. (*Left*) γ distribution of delays with different shape factors (k = 1, 5, and 20) and the same mean (τ = 8 ms). (*Right*) Synchronization index at zero lag of the outer neurons as a function of the shape factor and mean of the distribution of delays.

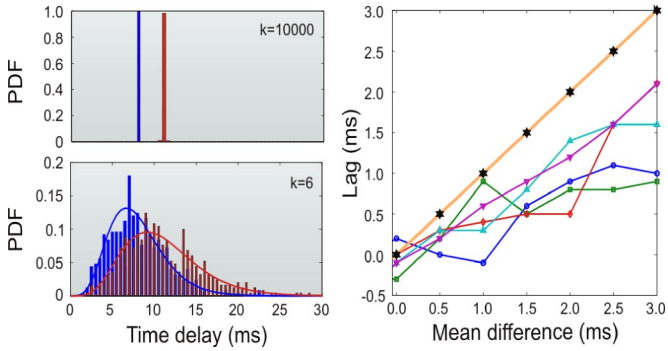

Fig. 4. Effects of dissimilar distributions of axonal delays on the lag of synchronization. (*Left*) different γ distributions of delays used for the 2 dissimilar branches of the network module. (*Upper*) Distributions with shape factor k = 10,000 (quasi-δ) and means of 8 and 11 ms. (*Lower*) Distributions with shape factor k = 6 and means of 8 and 11 ms. (*Right*) Lag between the discharges of the outer neurons as a function of the difference in the mean of the distributions of delays for the 2 branches. Shape factors k = 6 (squares), k = 8 (circles), k = 10 (diamonds), k = 12 (upright triangles), k = 14 (inverted triangles), and k = 10,000 (stars) were tested.

nature of the relay cell. The results indicate that when a relay cell was operating in a parameter regime different from the outer ones (such as different firing rate or conductances), the zero lag synchrony among them was not disturbed. Remarkably, even in the case where the relay cell was operating in a subthreshold regime, and thus only spiking because of the excitatory input from any of the outer neurons, the process of self-organization toward the zero lag synchrony was observed. It is worth mentioning that in all cases such firing synchronization is achieved through small shifts in the spiking latencies that left the mean frequency of discharges (rate) almost unchanged (the largest variations observed were smaller than a 9% relative change).

Dynamical Relaying-Based Synchronization Is Robust to Broad Distributions of Axonal Delays. The axons that form cortico–cortical or thalamo–cortical fibers differ in diameter, myelin thickness, and internodal distance. The variability from 1 axon to another of these characteristics affects the speed of propagation of action potentials and eventually translates into the existence of a whole range of latencies in the neuronal communication between separate brain areas. Thus, conduction times along fibers are more suitably considered as a spectrum rather than a single latency value (16, 34). To tackle this issue we modeled the dispersion of axonal latencies by assuming that individual temporal delays of the arrivals of action potentials (i.e., latency times) follow a γ distribution (see Eq. **S13** in the *SI Materials and Methods*). This mimicked the variability among the different axons connecting 2 pools of neurons. Because data about axonal distributions of conduction velocities in long-range fibers is limited (16, 34), and there is probably not a unique prototypical form of such distributions we decided to explore a whole family of γ distributions with different shapes. Fig. 3 *Left* illustrates different γ distributions of axonal delays for 3 different shape factors.

Our numerical simulations indicate that for a large region of mean delays (between 3 and 10 ms), the outer neurons synchronize independently of the shape of the distribution. These results can be observed in Fig. 3 *Right*, where we plot the zero lag synchronization index of the outer neurons of the network motif as a function of the shape of the γ distribution of axonal delays and its mean value. Only distributions with unrealistic small shape factor (i.e., exponentially decaying distributions) prevent synchrony irrespective of the average delay of the synaptic connections. For more realistic distributions, there is an extensive region of axonal delays that gives rise to the zero lag synchrony among the outer neurons. As in the case of single latencies, we found a drop in the synchronization quality for distributions with a mean value of approximately $\tau \approx$10–12 ms, where chaotic firing is observed. The isochronous spiking coherence is in general recovered for larger mean delay values.

Up until now, we have considered similar distributions of axonal delays in each of the 2 branches connecting the relay neuron to the outer units. This holds when the relay cell occupies a location that is approximately equidistant from the outer elements. Nevertheless, we also investigated the situation in which the axonal delays of each of the 2 pathways of the network motif are described by dissimilar distributions. In those cases, we have found that if the distributions of delays for each branch of the module have different mean values then a nonzero phase lag appears between the dynamics of the outer neurons. This effect is illustrated in Fig. 4. For δ distributions of delays (which is equivalent to the single latency case) the lag amounts to the delay difference that is still much smaller than the sum of the delays accumulated to communicate both neurons. When studying the effect of broader distributions of delays, we observed that outer cells tend to fire with a lag even smaller than the difference in the mean values of the distributions. Thus, broad distributions of delays allow distant neurons to fire at almost zero lag even when the mean delay values of the branches differed in several milliseconds.

Populations of Distant Neurons Can Also Exhibit Zero Lag Synchrony via Dynamical Relaying. A further key step in demonstrating the feasibility of synchronizing widely separated neurons via dynamical relaying is the extension of the previous results to the level of neuronal populations, the scale at which neuronal microcircuits develop their function (35). Far from being independent, the dynamical response of any neuron is massively affected by the activity of the local network of cells or functional unit into which it is embedded and by the long-range afferents originating in distant populations. It is also important to consider the random-like influences usually referred to as background noise, a term that collects a variety of processes from spontaneous release of neurotransmitters to fluctuations of unspecific inputs (36, 37). In such a scenario, we explored whether long-range fibers supporting dynamical relaying, and thus indirectly connecting pools of neurons, are suitable to act as the driving force promoting remote interpopulation synchrony in the presence of local interactions and noise sources.

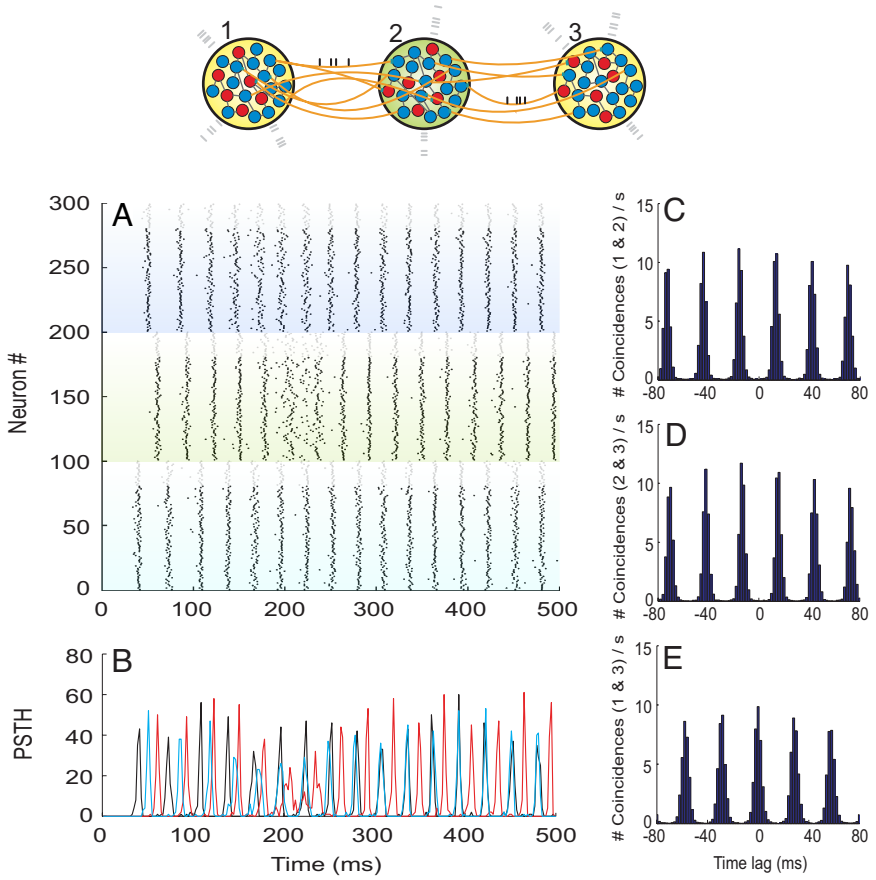

Fig. 5. Dynamics of 3 large-scale networks interacting through dynamical relaying. (*A*) Raster plot of 300 neurons randomly selected among the 3 populations (neurons 1–100 are from population 1, 101–200 from population 2, and 201–300 from population 3). The top 20 neurons of each subpopulation (plotted in gray) are inhibitory, and the rest are excitatory (black). (*B*) Firing histogram of each subpopulation of 100 randomly selected neurons (black, red, and blue colors code for populations 1, 2, and 3, respectively). (*C*) Averaged cross-correlogram between neurons of populations 1 and 2. (*D*) Averaged cross-correlogram between neurons of populations 2 and 3. (*E*) Averaged cross-correlogram between neurons of populations 1 and 3. At t = 100 ms, the external interpopulation synapses become active. Bin sizes for the histogram and correlograms are set to 2 ms. Interpopulation axonal delays are set to 12 ms.

To check whether zero lag-correlated firing is thus induced among neurons in different populations, we built 3 large networks of sparsely connected excitatory and inhibitory IAF neurons (see *Materials and Methods* and *SI Materials and Methods*). We interconnected the 3 populations following the topology of the network motif under study, i.e., the mutual relaying of activities of 2 external populations onto an intermediate pool of relay neurons.

We first initialized all 3 networks without the long-range interpopulation connections. Only the recurrent local connections and the Poissonian external background were active and thus responsible for any dynamics in the stand-alone networks. Consequently, each population initially exhibited spiking of their neurons in an incoherent and unsynchronized fashion with respect to neurons belonging to any of the other populations. Once the long-range synapses were activated, we observed that the firing of the neurons organized toward the collective synchrony of the outer populations. Fig. 5 illustrates the typical raster plot, firing histogram, and cross-correlograms of neurons among the 3 interconnected networks for a conduction delay of 12 ms. Similar results were observed when we explored other axonal delays in the range of 2–20 ms. The mean period of the coupled oscillatory activity (≈32 ms) was found to be close to the local rhythm of the isolated networks (≈34 ms), and therefore the coupling had little effect on the frequency of oscillation. A different situation might appear when the populations are tuned so that no prominent oscillatory activity emerges in the isolated networks before they are functionally coupled. In that case, we found from our model that the reciprocal coupling among the networks can act as a generator of oscillations and zero lag synchrony. In the latter case, however, we found a periodicity strongly influenced by the conduction delay times.

To determine the role of the relay cells (population 2) in shaping the synchronization among cells belonging to the remote neuronal networks (populations 1 and 3), we designed the following control experiment. We investigated the neuronal dynamics obtained under exactly the same conditions as in the former approach with the only variation that this time the 2 outer networks interacted directly. The results are summarized in Fig. 6. The sole change of the topology of the connections meant that networks 1 and 3, even if engaged in oscillations with similar characteristics as before, no longer synchronized their spikes at zero lag.

Discussion

In the previous paragraphs we introduced a network topology that enhances the zero lag synchronization of distant populations of neurons. Specifically, we showed that 2 populations of cells can become synchronized with zero phase lag if coupled reciprocally to a third population. Synchrony is maintained even when the fibers connecting the networks accumulate axonal delays of several tens of milliseconds. This suggests that such topology may contribute to the large-scale synchronization phenomena reported in a number of experiments during the last 2 decades (10, 15).

In this context, R. Llinás and other authors have suggested the reciprocal coupling of cortical areas with the thalamus as a mechanism to support distributed cortical processing and the emergence of consciousness (38–40). Edward G. Jones and other authors have explicitly proposed the dispersed cortical projections of matrix cells in the dorsal thalamic nuclei together with the layer V corticothalamic projection as the appropriate circuitry to extend thalamocortical activity and to form a substrate for synchronization of widespread ensembles of cortical and thalamic cells (29, 30). The resemblance of such circuitry with the topology studied here is evident once the identification of the associative nuclei of the thalamus as our relay population

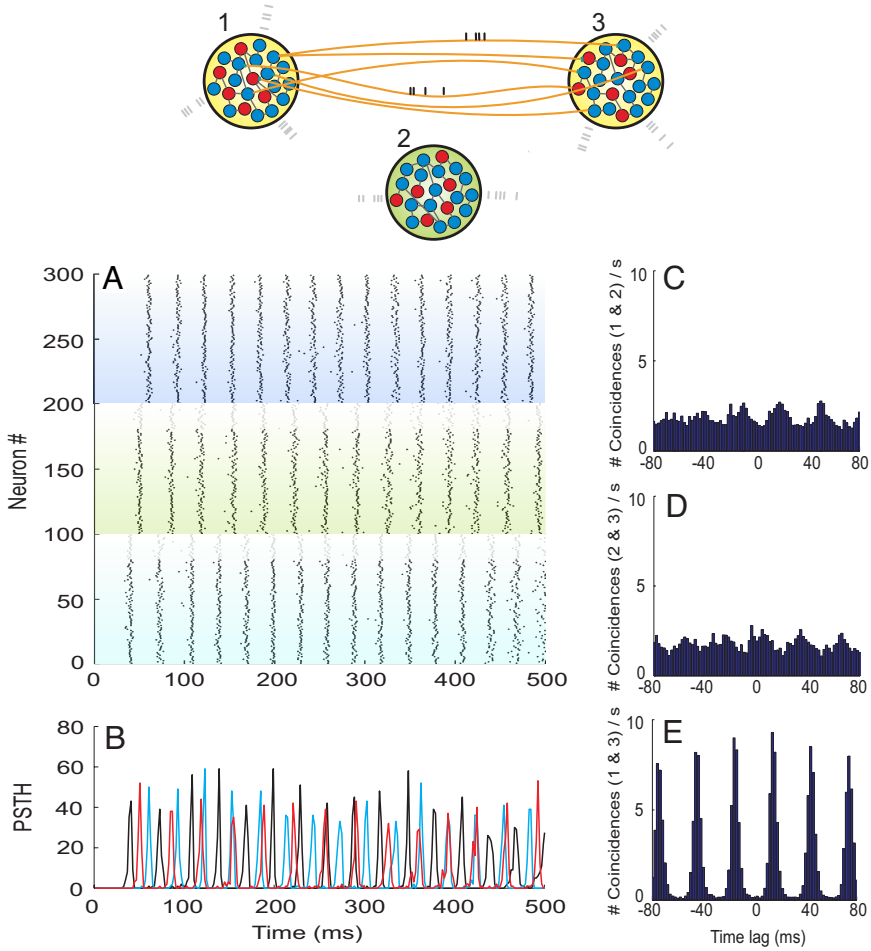

Fig. 6. Dynamics of 2 large-scale networks interacting directly. Population 2 is disconnected from other populations. Structure of the panels and parameters are otherwise as in Fig. 5.

for cortical activity is performed. However, the principal message of our results is not the identification of the physiological structures potentially responsible for long-range cortical synchrony but to show that the long latencies associated with cortico–thalamo–cortical loops are compatible with synchronization across large distances. Coherent oscillations between remote cortical populations can of course be generated also by reciprocally coupling these areas to other cortical areas or other subcortical structures. In fact, the aggregation of several of such motifs around a putative hub (forming a star-like network with the center unit playing the role of the relay element) also favors satellite nodes to spike in zero lag synchrony (41).

The most important requirement for zero phase lag synchronization is that the relay population of cells occupies a temporally equidistant location from the pools of neurons to be synchronized. It is significant to point out that recent studies have identified a constant temporal latency between thalamic nuclei and almost any area in the mammalian neocortex (42). Thus, in this scheme, thalamic nuclei occupy a central position for the mediation of zero phase solutions.

In general, it is quite probable that a variety of mechanisms are responsible for bringing synchrony at different levels (distinguishing for example, among local and long-distance synchrony) and different cerebral structures. The fact that each thalamus projects almost exclusively ipsilaterally (the massa intermedia is clearly inadequate for supporting the required interthalamic communication) is already an indication that the callosal commissure should play a prominent role in facilitating interhemispheric coherence. Lesion studies have since long confirmed this view (17). However, within a single hemisphere the disruption of intracortical connectivity by a deep coronal cut through the suprasylvian gyrus was observed not to disturb the synchrony of spindle oscillations across regions of cortex located at both sides of the lesion (6). This finding suggests that subcortical, and in particular cortico–thalamic interactions, could be responsible for maintaining both the long-range cortical and thalamic coherence found in such a regime. It is likely that subcortical loops with widespread connectivity such as the associative or nonspecific cortico–thalamo–cortical circuits could run in parallel as an alternative pathway for the large-scale integration of cortical activity within a single hemisphere (30, 35, 40, 43). As we have shown here, with such connectivity pattern even large axonal conduction delays represent no detriment to the observation of zero time lag synchronization. It is also important to remark that connectivity studies in primate cortex have identified the pattern of connections studied here as the most frequently repeated motif at the level of cortico–cortical connections in the visual cortex (44–46). The functional relevance of this topology of cortical network is unclear but according to our results is ideally suited to sustain coherent activity.

In summary, the network motif highlighted here has the property of naturally inducing zero lag synchrony among the firing of 2 separated neuronal populations. The associative thalamic nuclei have the cortex as their main input and output sources and seem to represent active relay centers of cortical activity with properties well suitable for enhancing cortical coherence (30). From the experimental side, the relatively well-controlled conditions of brain slice experiments, allowing for the identification of synaptically coupled neurons and cell type, might be a first step for testing whether the topology

investigated here provides a significant substrate for coherent spiking activity. Another important issue is how the dynamic selection of the areas that engage and disengage into synchrony is achieved. It has been hypothesized that a dynamically changing coherent activity pattern may ride on top of the anatomical structure to provide flexible neuronal communication pathways (47). Based on the properties formerly reviewed, subcortical structures such as some thalamic nuclei might be promising candidates to play a role in regulating such coherence and contribute to the large-scale cortical communication.

Materials and Methods

Two neuronal models were numerically simulated to test the synchronization properties of the neuronal circuits investigated here.

In the most simplified version of the neuronal motif we focused on the dynamics of 2 single-compartment neurons that interact with each other via reciprocal synaptic connections with an intermediate third neuron of the same type (see Fig. 1 *Top*). The dynamics of the membrane potential of each neuron was modeled by the classical HH equations (48) plus the inclusion of appropriate delayed synaptic currents that mimic the chemical interaction between nerve cells.

The second class of models we have considered consists of 3 large balanced populations of IAF neurons (49). Fig. 5 *Upper* is a sketch of the connectivity. Each network consisted of 4,175 IAF neurons of which 80% were excitatory. The internal synaptic connectivity was chosen to be random, i.e., each neuron synapsed with 10% of randomly selected neurons within the same population, such that the total number of synapses in each network amounted to ≈1,700,000 contacts. In additional to model background noise, each neuron was subjected to the influence of an external train of spikes with a Poissonian profile. The interpopulation synaptic links were arranged such that each neuron in any population receives input from 0.25% of the excitatory neurons in the neighboring population. Note that the interpopulation links remained small in number compared with the local coupling that allows to consider the system as 3 weakly interacting networks of neurons rather than a single homogeneous network. Intrapopulation axonal delays were set to 1.5 ms, whereas the fibers connecting different populations were assumed to involve much longer latencies to mimic the long-range character of such links.

Parameters, evolution equations, simulation schemes, and data analysis for these 2 models are detailed in the *SI Materials and Methods*.

ACKNOWLEDGMENTS. We thank Wolf Singer, Christopher J. Honey, and Nancy Kopell for the careful reading of the manuscript and helpful discussions. R. V. and G. P. also thank Carl van Vreeswijk and Victor Eguiluz for fruitful discussions. This work was supported by the Hertie Foundation, European Commission Project GABA (FP6-NEST Contract 043309), and the Spanish MCyT and Feder under Project FISICO (FIS-2004-00953).

1. Gray CM, Konig P, Engel AK, Singer W (1989) Oscillatory responses in cat visual cortex exhibit intercolumnar synchronization which reflects global stimulus properties. *Nature* 338:334–337.
2. Engel AK, Kreiter AK, Konig P, Singer W (1991) Synchronization of oscillatory neuronal responses between striate and extrastriate visual cortical areas of the cat. *Proc Natl Acad Sci USA* 88:6048–6052.
3. Castelo-Branco M, Goebel R, Neuenschwander S, Singer W (2000) Neuronal synchrony correlates with surface segregation rules. *Nature* 405:685–689.
4. Tiesinga P, Fellows JM, Sejnowski T (2008) Regulation of spike timing in visual cortical circuits. *Nat Rev Neurosci* 9:97–109.
5. Traub RD, Whittington MA, Stanford IM, Jefferys JGR (1996) A mechanism for generation of long-range synchronous fast oscillations in the cortex. *Nature* 383:621–624.
6. Contreras D, Destexhe A, Sejnowski TJ, Steriade M (1996) Control of spatiotemporal coherence of a thalamic oscillation by corticothalamic feedback. *Science* 274:771–774.
7. Roelfsema PR, Engel AK, Konig P, Singer W (1997) Visuomotor integration is associated with zero time lag synchronization among cortical areas. *Nature* 385:157–161.
8. Fries P, Roelfsema PR, Engel AK, Konig P, Singer W (1997) Synchronization of oscillatory responses in visual cortex correlates with perception in interocular rivalry. *Proc Natl Acad Sci USA* 94:12699–12704.
9. Rodriguez E, *et al.* (1999) Perception's shadow: Long-distance synchronization of human brain activity. *Nature* 397:430–433.
10. Varela FJ, Lachaux JP, Rodriguez E, Martinerie J (2001) The brainweb: Phase synchronization and large-scale integration. *Nat Rev Neurosci* 2:229–239.
11. Konig P, Engel AK, Singer W (1995) Relation between oscillatory activity and long-range synchronization in cat visual cortex. *Proc Natl Acad Sci USA* 92:290–294.
12. von Stein A, Chiang C, Konig P (1997) Top-down processing mediated by interareal synchronization. *Proc Natl Acad Sci USA* 97:14748–14753.
13. Soteropoulus DS, Baker SN (2006) Cortico-cerebellar coherence during a precision grip task in the monkey. *J Neurophysiol* 95:1194–1206.
14. Witham CL, Wang M, Baker SN (2007) Cells in somatosensory areas show synchrony with β oscillations in monkey motor cortex. *Eur J Neurosci* 26:2677–2686.
15. Singer W (1999) Neuronal synchrony: A versatile code for relations? *Neuron* 24:49–65.
16. Ringo JL, Doty RW, Demeter S, Simard PY (1994) Time is the essence: A conjecture that hemispheric specialization arises from interhemispheric conduction delay. *Cerebr Cortex* 4:331–343.
17. Engel AK, Kreiter AK, Konig P, Singer W (1991) Interhemispheric synchronization of oscillatory neuronal responses in cat visual cortex. *Science* 252:1177–1179.
18. Ritz R, Gestner W, Fuentes U, van Hemmen JL (1994) A biologically motivated and analytically soluble model of collective oscillations in the cortex. II. Applications to binding and pattern segmentation. *Biol Cybernet* 71:349–358.
19. Sirovich L, Omurtag A, Lubliner K (2006) Dynamics of neural populations: Stability and synchrony. *Networks* 17:3–29.
20. van Vreeswijk C, Abbott LF, Ermentrout GB (1994) When inhibition not excitation synchronizes neural firing. *J Comput Neurosci* 1:313–321.
21. Kopell N, Ermentrout GB (2004) Chemical and electrical synapses perform complementary roles in the synchronization of interneuronal networks. *Proc Natl Acad Sci USA* 101:15482–15487.
22. Ermentrout GB, Kopell N (1998) Fine structure of neural spiking and synchronization in the presence of conduction delays. *Proc Natl Acad Sci USA* 95:1259–1264.
23. Kopell N, Ermentrout GB, Whittington MA, Traub RD (1998) Gamma rhythms and beta rhythms have different synchronization properties. *Proc Natl Acad Sci USA* 97:1867–1872.
24. Knoblauch A, Sommer FT (2003) Synaptic plasticity, conduction delays, and interareal phase relations of spike activity in a model of reciprocally connected areas. *Neurocomputing* 52–54:301–306.
25. Swindale NV (2003) Neural synchrony, axonal path lengths, and general anesthesia: A hypothesis. *Neuroscientist* 9:440–445.
26. D'Huys O, Vicente R, Erneux T, Danckaert J, Fischer I (2008) Synchronization properties of network motifs: Influence of coupling delay and symmetry. *Chaos* 18:037116.
27. Fischer I, *et al.* (2006) Zero-lag long-range synchronization via dynamical relaying. *Phys Rev Lett* 97:123902.
28. Vicente R, Fischer I, Mirasso CR (2007) Simultaneous bidirectional message transmission in a chaos-based communication scheme. *Optics Lett* 32:403.
29. Jones EG (2002) Thalamic circuitry and thalamocortical synchrony. *Phil Trans R Soc London Ser B* 357:1659–1673.
30. Shipp S (2003) The functional logic of cortico-pulvinar connections. *Phil Trans R Soc London Ser B* 358:1605–1624.
31. Ermentrout JB (1996) Type I membranes, phase resetting curves, and synchrony. *Neural Comput* 8:979–1001.
32. Reyes AD, Fetz EE (1993) Two modes of interspike interval shortening by brief transient depolarizations in cat neocortical neurons. *J Neurophysiol* 69:1661–1672.
33. Reyes AD, Fetz EE (1993) Effects of transient depolarizing potentials on the firing rate of cat neocortical neurons. *J Neurophysiol* 69:1673–1683.
34. Aboitiz F, Scheibel AB, Fisher RS, Zaidel E (1992) Fiber composition of the human corpus callosum. *Brain Behav Evol* 598:143–153.
35. Douglas RJ, Martin KAC (2004) Neuronal circuits of the neocortex. *Annu Rev Neurosci* 27:419–451.
36. Pare D, Shink E, Gaudreau H, Destexhe A, Lang EJ (1998) Impact of spontaneous synaptic activity on the resting properties of cat neocortical pyramidal neurons in vivo. *J Neurophysiol* 78:1450–1460.
37. Arieli A, Sterkin A, Grinvald A, Aertsen A (1996) Dynamics of ongoing activity: Explanation of the large variability in evoked cortical responses. *Science* 273:1868–1871.
38. Llinas RR, Pare D (1997) Coherent oscillations in specific and nonspecific thalamocortical networks and their role in cognition. *Thalamus* (Elsevier, Amsterdam), Vol 2, pp 501–516.
39. Llinas RR, Ribary U, Contreras D, Pedroarean C (1998) The neuronal basis for consciousness. *Phil Trans R Soc London Ser B* 353:1841–1849.
40. Sherman SM, Guillery RW (2002) The role of the thalamus in the flow of information to the cortex. *Phil Trans R Soc London Ser B* 357:1695–1708.
41. Sporns O, Honey CJ, Kotter R (2007) Identification and classification of hubs in brain networks. *PLoS ONE* 2:e1049.
42. Salami M, Itami C, Tsumoto T, Kimura F (2003) Change of conduction velocity by regional myelination yields to constant latency irrespective of distance between thalamus to cortex. *Proc Natl Acad Sci USA* 100:6174–6179.
43. Slotnick SD, Moo LR, Kraut MA, Lesser RP, Hart J (2002) Interactions between thalamic and cortical rhythms during semantic memory recall in human. *Proc Natl Acad Sci USA* 99:6440–6443.
44. Sporns O, Kotter R (2004) Motifs in brain networks. *PLoS Biol* 2:e369.
45. Sporns O, Chialvo D, Kaiser M, Hiltetag CC (2004) Organization, development, and function of complex brain networks. *Trends Cognit Sci* 8:418–425.
46. Honey CJ, Kotter R, Breakspear M, Sporns O (2007) Network structure of cerebral cortex shapes functional connectivity on multiple time scales. *Proc Natl Acad Sci USA* 104:10240–10245.
47. Fries P (2005) A mechanism for cognitive dynamics: Neuronal communication through neuronal coherence. *Trends Cognit Sci* 9:474–480.
48. Hodgkin AL, Huxley AF (1952) A quantitative description of the membrane current and its application to conduction and excitation in nerve. *J Physiol* 117:500–544.
49. Brunel N (2000) Dynamics of sparsely connected networks of excitatory and inhibitory spiking neurons. *J Comput Neurosci* 8:183–208.

Supporting Information

Vicente *et al.* 10.1073/pnas.0809353105

SI Materials and Methods

Models. For the first class of models investigated, we have simulated the dynamics of three reciprocally coupled single-compartment Hodgkin and Huxley (HH) neurons arranged as in the configuration shown in Fig. 1 of the main text. The temporal evolution of the voltage across the membrane of each neuron is given by

$$C\frac{dV}{dt} = -g_{Na}m^3h(V-E_{Na}) - g_K n^4(V-E_k) - g_L(V-E_L) + I_{ext} + I_{syn}, \quad [S1]$$

where $C = 1\ \mu\text{F/cm}^2$ is the membrane capacitance, the constants $g_{Na} = 120\ \text{mS/cm}^2$, $g_K = 36\ \text{mS/cm}^2$, and $g_L = 0.3\ \text{mS/cm}^2$ are the maximal conductances of the sodium, potassium, and leakage channels, and $E_{Na} = 50$ mV, $E_K = -77$ mV, and $E_L = -54.5$ mV stand for the corresponding reversal potentials. According to HH formulation, the voltage-gated ion channels are described by the following set of differential equations

$$\frac{dm}{dt} = \alpha_m(V)(1-m) - \beta_m(V)m, \quad [S2]$$

$$\frac{dh}{dt} = \alpha_h(V)(1-h) - \beta_h(V)h, \quad [S3]$$

$$\frac{dn}{dt} = \alpha_n(V)(1-n) - \beta_n(V)n, \quad [S4]$$

where the gating variables $m(t)$, $h(t)$, and $n(t)$ represent the activation and inactivation of the sodium channels and the activation of the potassium channels, respectively. The experimentally fitted voltage-dependent transition rates are

$$\alpha_m(V) = \frac{0.1(V+40)}{1-\exp(-(V+40)/10)}, \quad [S5]$$

$$\beta_m(V) = 4\exp(-(V+65)/18), \quad [S6]$$

$$\alpha_h(V) = 0.07\exp(-(V+65)/20), \quad [S7]$$

$$\beta_h(V) = [1+\exp(-(V+35)/10)]^{-1}, \quad [S8]$$

$$\alpha_n(V) = \frac{(V+55)/10}{1-\exp(-0.1(V+55))}, \quad [S9]$$

$$\beta_n(V) = 0.125\exp(-(V+65)/80). \quad [S10]$$

The synaptic transmission between neurons is modeled by a postsynaptic conductance change with the form of an α function

$$\alpha(t) = \frac{1}{\tau_d - \tau_r}(\exp(-t/\tau_d) - \exp(-t/\tau_r)), \quad [S11]$$

where the parameters τ_d and τ_r stand for the decay and rise time of the function and determine the duration of the response. Synaptic rise and decay times were set to $\tau_r = 0.1$ and $\tau_d = 3$ ms, respectively, for the simulations exhibited in *Results* in the main text. Other sets of values running from 0.1 to 7 ms were also tested for such time constants. Finally, the synaptic current takes the form

$$I_{syn}(t) = -\frac{g_{max}}{N}\sum_{\tau_l}\sum_{spikes}\alpha(t - t_{spike} - \tau_l)(V(t) - E_{syn}), \quad [S12]$$

where g_{max} (here fixed to 0.05 mS/cm^2) describes the maximal synaptic conductance, and the internal sum is extended over the train of presynaptic spikes occurring at t_{spike}. The delays arising from the finite conduction velocity of axons are taken into account through the latency time τ_l in the α function. Thus, the external sum covers the N different latencies that arise from the conduction velocities that different axons may have in connecting two neuronal populations. N was typically set to 500 in the simulations. For the single-latency case, all τ_l were set to the same value, whereas when studying the effect of a distribution of delays, we modeled such dispersion by a γ distribution with a probability density of

$$f(\tau_l) = \tau_l^{k-1}\frac{\exp(-\tau_l/\theta)}{\theta^k\Gamma(k)}, \quad [S13]$$

where k and θ are shape and scale parameters of the γ distribution. The mean time delay is given by $\hat{\tau}_l = k\theta$.

Excitatory and inhibitory transmissions were differentiated by setting the synaptic reversal potential to be $E_{syn} = 0$ mV or $E_{syn} = -80$ mV, respectively. An external current stimulation I_{ext} was adjusted to a constant value of 10 μA/cm^2. Under such conditions, a single HH-type neuron enters into a periodic regime, firing action potentials at a natural period of $T_{nat} = 14.66$ ms.

The second class of models we have considered consists of three large balanced populations of integrate and fire (IAF) neurons. Each population was composed of 4,175 IAF neurons from which ≈80% were excitatory. The local connectivity was sparse and random. Each neuron received thus a synapse from 10% of randomly selected cells inside its population and from 0.25% from the excitatory class of the neighboring populations. The voltage dynamics of each neuron was then given by the following equation

$$\tau_m\frac{dV_i}{dt} = -V_i(t) + RI_i(t), \quad [S14]$$

where τ_m stands for the membrane constant and $I(t)$ is a term collecting the currents arriving to the soma. The latter is decomposed in postsynaptic currents and external Poissonian noise

$$RI_i(t) = \tau_m\sum_j J_j\sum_k\delta(t - t_j^k - \tau_l) + A\xi_i, \quad [S15]$$

where J_j is the postsynaptic potential amplitude, $t_j^k$is the emission time of the kth spike at neuron j, and τ_l is the transmission axonal delay. The external noise ζ_i is simulated by subjecting each neuron to the simultaneous input of 1,000 independent homogeneous Poissonian action potential trains with an individual rate of 5 Hz. Different cells were subjected to different realizations of the Poissonian processes to ensure the independence of noise sources for each neuron. J_{exc} and A amplitudes were set to 0.1 mV. The balance of the network was controlled by setting $J_{inh} = -\text{g}J_{exc}$, with g ranging from 3.5 to 4 to compensate the outnumbering of excitatory units.

The dynamics of each neuron evolved from the reset potential of $V_r = 10$ mV by means of the synaptic currents up to the time when the potential of the ith neurons reached a threshold of 20 mV, a value at which the neuron fires and its potential relaxes to V_r. The

potential is clamped then to this quantity for a refractory period of 2 ms during which no event can perturb this neuron.

Simulations. The set of Eq. **S1–S12** was numerically integrated using the Heun method with a time step of 0.02 ms. For the first class of models we investigated, i.e., the three HH cells neuronal circuit, we proceeded as follows. Starting from random initial conditions, each neuron was first simulated without any synaptic coupling for 200 ms, after which frequency adaptation occurred, and each neuron settled into a periodic firing regime with a well-defined frequency. The relation between the phases of the oscillatory activities of the neurons at the end of this warm-up time was entirely determined by the initial conditions. After this period and once the synaptic transmission was activated, a simulation time of 3 s was recorded. This allowed us to trace the change in the relative timing of the spikes induced by the synaptic coupling in this neural circuit.

The second class of model involving the interaction of heterogeneous large populations of neurons was built with the neuronal simulator package NEST (1). The simulation of such networks uses a precise time-driven algorithm with the characteristic that the spike events are not constrained to the discrete time lattice. In a first stage of the simulation the three populations were initialized being isolated from each other and let them to evolve just due to their internal local connectivity and external Poissonian noise. In a subsequent phase, the three populations were interconnected according to the motif investigated here and simulated during 1 s.

Data Analysis. The strength of the synchronization and the phase difference between each individual pair of neurons (m, n) were derived for the first model of three HH neurons by the computation of the order parameter defined as

$$\rho(t) = \frac{1}{2}\left|\exp(i\phi_m(t)) + \exp(i\phi_n(t))\right|, \qquad \textbf{[S16]}$$

which takes the value of 1 when two systems oscillate in-phase and 0 when they oscillate in an antiphase regime or in an uncorrelated fashion. To compute this quantifier, it is only necessary to estimate the phases of the individual neural oscillators. An advantage of this method is that one can easily reconstruct the phase of a neuronal oscillation from the train of spikes without the need of recording the full membrane potential time series (2). The idea behind this is that the time interval between two well-defined events (such as action potentials) defines a complete cycle, and the phase increase during this time amounts to 2π. Then, linear interpolation is used to assign a value to the phase between the spike events.

The synchrony among the large populations of neurons of the second model studied in the article was assessed by the computation of averaged cross-correlograms. For that purpose, we randomly selected three neurons (one from each of the three populations) and computed for each pair of neurons belonging to different populations the histogram of coincidences (bin size of 2 ms) as a function of the time shift of one of the spike trains. We computed the cross-correlograms within the time window ranging from 500 to 1,000 ms to avoid the transients toward the synchronous state. The procedure was repeated 300 times to give rise to the estimated averaged distributions of coincidences exhibited in Figs. 5 and 6 in the main text.

Stability Computations. In this section, we follow an analytical approach to compute the stability of the zero lag synchronization of outer neurons interacting through a dynamical relaying element (see the motif shown in Fig. 1 *Top* in the main text). In particular, we demonstrate that the stability of such solution extends over larger regions of the axonal delay parameter than for the case of only two neurons interacting directly. These calculations are performed under the phase reduction approximation of the spiking dynamics of neurons, which assume that the oscillatory activity of each neuron can be described by a phase variable.

The dynamics of each cell in the motif is then described as

$$\frac{d\theta_i}{dt} = \frac{1}{T_i} + \sum_{n,k} a_{i,k}\delta(t - t_k^n - \tau)\Delta(\theta_i), \qquad \textbf{[S17]}$$

where θ_i is the phase of each neuron within its spiking cycle, T_i amounts to the natural period, $a_{i,k}$ is the strength of the interaction between neurons, and t_k^n represents the time of the nth spike of the kth neuron (3). The axonal delay in the communication between the neurons is taken into account by the temporal latency τ. The pulse-coupled interaction among the neurons is captured by the phase response curve (PRC) $\Delta(\theta)$. This curve characterizes the change in the cycle period (phase shift) of an oscillator induced by a perturbation as a function of the timing at which it is received. It is defined as

$$\Delta(\theta) \equiv 1 - \frac{T^*(\theta)}{T}, \qquad \textbf{[S18]}$$

where T^* is the new period of the oscillation induced by a perturbation injected at the phase θ. PRCs of neurons and many other biological oscillators have been measured experimentally as well as computed for models and provide a rigorous framework to predict the dynamical properties of spiking neurons (4, 5). A recent example of the use of the PRC method in small networks of biological neurons can also be found in ref. 6.

Once we establish the basic equations for the pulse-coupled interaction among neurons, we proceed by computing the possible phase locked states. Before that step we change first the reference system of our phase variables by defining the new phase φ such that $\theta \equiv \nu t + \varphi(t)$, with $\nu = 1/T$. Assuming identical natural periods of the cells ($\nu_1 = \nu_2 = \nu_3 = \nu$), Eq. **S17** is rewritten for the motif of three neurons interacting through dynamical relaying as

$$\begin{aligned}
\frac{d\varphi_1}{dt} &= a_{1,2}\sum_n \delta(t - t_2^n - \tau)\Delta(\nu t + \varphi_1),\\
\frac{d\varphi_2}{dt} &= a_{2,1}\sum_n \delta(t - t_1^n - \tau)\Delta(\nu t + \varphi_2)\\
&\quad + a_{2,3}\sum_n \delta(t - t_3^n - \tau)\Delta(\nu t + \varphi_2),\\
\frac{d\varphi_3}{dt} &= a_{3,2}\sum_n \delta(t - t_2^n - \tau)\Delta(\nu t + \varphi_3). \qquad \textbf{[S19]}
\end{aligned}$$

Following ref. 3 in the weak coupling case, one can approximate the nth spiking time of each neuron as $t_i^n \approx \dfrac{n - \varphi_i}{\nu}$. Substituting this expression in Eq. **S19** and averaging the instantaneous coupling over a full period of the oscillation results in

$$\begin{aligned}
\frac{d\varphi_1}{dt} &= a_{1,2}\Delta(\varphi_1 - \varphi_2 + \nu\tau),\\
\frac{d\varphi_2}{dt} &= a_{2,1}\Delta(\varphi_2 - \varphi_1 + \nu\tau) + a_{2,3}\Delta(\varphi_2 - \varphi_3 + \nu\tau),\\
\frac{d\varphi_3}{dt} &= a_{3,2}\Delta(\varphi_3 - \varphi_2 + \nu\tau). \qquad \textbf{[S20]}
\end{aligned}$$

Phase-locked solutions take the form $\varphi_i(t) = \Omega t + \phi_i$, with ϕ_i being a constant. The existence of the zero phase lag solution between the outer neurons ($\phi_1 = \phi_3$) requires the following conditions being satisfied simultaneously

$$a_{1,2} = a_{3,2},$$

$$(a_{2,1} + a_{2,3})\Delta(\phi_2 - \phi_1 + \nu\tau) = a_{1,2}\Delta(\phi_1 - \phi_2 + \nu\tau). \quad \textbf{[S21]}$$

For simplicity, we consider the case where synaptic strength is normalized by the number of afferent inputs of each neuron so that the total coupling strength per neuron is the same ($a_{2,1} + a_{2,3} = a_{1,2} \equiv a$). In such case, the second condition is simply $\Delta(\phi_2 - \phi_1 + \nu\tau) = \Delta(\phi_1 - \phi_2 + \nu\tau)$. This condition can have multiple solutions depending on the specific PRC of the neuron class that we are interested in. In any case, two important solutions that hold for any PRC are $\phi_1 - \phi_2 = 0$ and $\phi_1 - \phi_2 = 1/2$. These solutions are the in-phase and antiphase relations for nearest neighbors oscillators.

A linear stability analysis for perturbations of the phase-locked solutions ($\varphi_i = \Omega t + \phi_i + \delta\phi_i$) gives rises to the system

$$\frac{d\delta\phi_1}{dt} = a\Delta'(\phi_1 - \phi_2 + \nu\tau)(\delta\phi_1 - \delta\phi_2),$$

$$\frac{d\delta\phi_2}{dt} = \frac{a}{2}\Delta'(\phi_2 - \phi_1 + \nu\tau)(2\delta\phi_2 - \delta\phi_1 - \delta\phi_3),$$

$$\frac{d\delta\phi_3}{dt} = a\Delta'(\phi_1 - \phi_2 + \nu\tau)(\delta\phi_3 - \delta\phi_2), \quad \textbf{[S22]}$$

where $'$ stands for the derivative operator. The eigenvalues of the characteristic equation are $\lambda_1 = a[\Delta'(\phi_1 - \phi_2 + \nu\tau) + \Delta'(\phi_2 - \phi_1 + \nu\tau)]$, $\lambda_2 = 0$, and $\lambda_3 = a\Delta'(\phi_1 - \phi_2 + \nu\tau)$ for the corresponding eigenvectors $\bar{V}_1 = [1, -\Delta'(\varphi_2 - \varphi_1 + \nu\tau)/\Delta'(\varphi_1 - \varphi_2 + \nu\tau), 1]$, $\bar{V}_2 = (1,1,1)$, and $\bar{V}_3 = (-1,0,1)$. For the in-phase and antiphase nearest-neighbors relations, the stability condition of the negativity of the eigenvalues reduces to the cases of $a\Delta'(\nu\tau) < 0$ and $a\Delta'(1/2 + \nu\tau) < 0$, respectively. The main role of the delay in this simplified description of the neuronal dynamics is to shift the phase at which a neuron receives the perturbation from the other neurons, which can substantially modify the stability of the solutions.

It is important to notice that for two directly coupled neurons, the zero phase lag synchronization exclusively corresponds to the in-phase nearest-neighbor relation. However, for the case of three neurons interacting as arranged in a bidirectional chain, both the nearest-neighbor in-phase and antiphase relations result in a zero phase solution for the outer neurons in the motif. This allows the outer neurons to fire isochronously for such delays where any of the two nearest-neighbor phase relations are stable and thus increases the delay range over which zero phase synchrony can appear. The precise range of stability must be computed specifically for each type of PRC according to the former stability criterion, but a general result is that such range is larger for the network motif under study than for the direct coupling of two neurons. In fact, when computing the phase relation for nearest neighbors in the full HH model of three neurons interacting through dynamical relaying, we could observe how this relation strongly varies as a function of the axonal delay (see Fig. S1). For some delays, the nearest-neighbor neurons were in-phase, but varying the delay they were observed to enter into states in which the antiphase solution dominated. For only two directly coupled neurons such changes limited the range of delays for which they could synchronize without any lag. However, the phase relation between the outer neurons 1 and 3 in the relaying motif was unsensitive to such sudden changes in the nearest-neighbor phase relation and remained in a zero lag solution for almost all explored delays up to 30 ms.

1. Brette R, *et al.* (2007) Simulation of networks of spiking neurons: A review of tools and strategies. *J Comp Neurosci* 23:349–398.
2. Pikovsky A, Rosemblum M, Kurths J (2002) *Synchronization: A Universal Concept in Nonlinear Science* (Cambridge Univ Press, Cambridge, UK).
3. Goel P, Ermentrout B (2002) Synchrony, stability, and firing patterns in pulse-coupled oscillators. *Physica D* 163:191–216.
4. Hansel D, Mato G, Meunier C (1995) Synchrony in excitatory neural networks. *Neural Net* 7:307–337.
5. Galan R, Ermentrout GB, Urban NN (2005) Efficient estimation of phase-resetting curves in real neurons and its significance for neural-network modeling. *Phys Rev Lett* 94:158101.
6. Pervouchine DD, *et al.* (2006) Low dimensional maps encoding dynamics in the entorhinal cortex and hippocampus. *Neural Comp* 18:2617–2750.

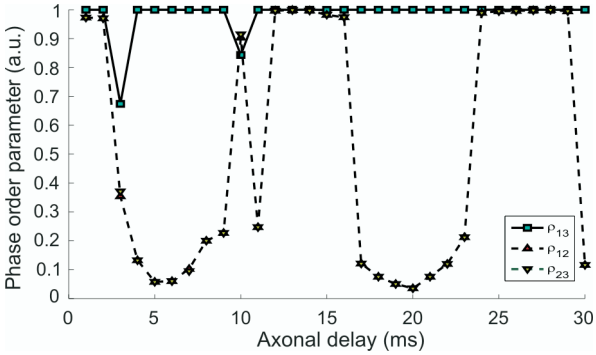

Fig. S1. Synchronization index at zero lag for pairs of HH neurons 1 and 3 (squares), 1 and 2 (upright triangles), and 2 and 3 (inverted triangles) as a function of the axonal delay. The coupling is excitatory, and the neurons are interacting according to the scheme in Fig. 1 *Top* in the main text. The sudden decays of the synchronization index between nearest neighbor neurons usually indicate the transitions to antiphase states. Notice that the zero-phase relation between neurons 1 and 3 is almost insensitive to such changes.